Molecular Simulations suggest Vitamins, Retinoids and Steroids as Ligands binding the Free Fatty Acid Pocket of SARS-CoV-2 Spike Protein

Deborah K Shoemark[1,2]*, Charlotte K. Colenso[3]*, Christine Toelzer[1,2], Kapil Gupta[1,2], Richard B. Sessions[1], Andrew D. Davidson[3], Imre Berger[1,2,4,5], Christiane Schaffitzel[1,2], James Spencer[3] and Adrian J. Mulholland[5].

*Joint first authors.

[1]School of Biochemistry, University of Bristol, 1 Tankard's Close, Bristol BS8 1TD, UK.

[2]Bristol Synthetic Biology Centre BrisSynBio, 24 Tyndall Ave, Bristol BS8 1TQ, UK.

[3]School of Cellular and Molecular Medicine, Biomedical Sciences Building, University of Bristol, Bristol, BS8 1TD, UK.

[4]Max Planck Bristol Centre for Minimal Biology, Cantock's Close, Bristol BS8 1TS, UK.

[5]School of Chemistry, University of Bristol, Bristol, BS8 1TS, United Kingdom.

Abstract

Following our recent identification of a fatty acid binding site in the SARS-CoV-2 spike protein (Toelzer *et al., Science* eabd3255 (2020)), we investigate the binding of linoleate and other potential ligands at this site using molecular dynamics simulations. The results support the hypothesis that linoleate stabilises the locked form of the spike, in which its interaction interface for the ACE2 receptor is occluded. The simulations indicate weaker binding of linoleate to the partially open conformation. Simulations of dexamethasone bound at this site indicate that it binds similarly to linoleate, and thus may also stabilize a locked spike conformation. In contrast, simulations suggest that cholesterol bound at this site may destabilize the locked conformation, and in the open conformation, may preferentially bind at an alternative site in the hinge region between the receptor binding domain and the domain below, which could have functional relevance. We also use molecular docking to identify potential ligands that may bind at the fatty acid binding site, using the Bristol University Docking Engine (BUDE). BUDE docking successfully reproduces the linoleate complex and also supports binding of dexamethasone at the spike fatty acid site. Virtual screening of a library of approved drugs identifies vitamins D, K and A, as well as retinoid ligands with experimentally demonstrated activity against SARS-CoV-2 replication *in vitro*, as also potentially able to bind at this site. Our data suggest that the fatty acid binding site of the SARS-CoV-2 spike protein may bind a diverse array of candidate ligands. Targeting this site with small molecules, including dietary components such as vitamins, which may stabilise its locked conformation and represents a potential avenue for novel therapeutics or prophylaxis for COVID-19.

Introduction

The global COVID-19 pandemic is caused by the SARS-CoV-2 coronavirus. Ten months since the first infections were reported, over 43 million people worldwide have become infected, with more than 1.15 million deaths in confirmed cases[1]. Initially thought to be a predominantly respiratory disease, its effects are not limited to the respiratory tract, and in severe cases extensive organ damage and death can result from e.g. a virus-induced cytokine storm[2]. Even in less severe cases of COVID-19, there is now evidence that infection can cause damage to heart muscle. In a recent study from Berlin[3], MRI scans of heart tissue of 100 recovered COVID-19 subjects found that 78 people, including those who had not been admitted to hospital, had sustained persistent heart damage, irrespective of the severity of their respiratory symptoms. Notwithstanding the small size of this study, and the as yet unknown extent of any tissue recovery, these findings suggest implications for reduced longevity in a 'COVID-recovered' population. Quality of life has also been adversely affected in the growing numbers of people described as suffering from 'long COVID', with some suffering neurological symptoms including fibromyalgia and profound fatigue, lasting for months after their initial illness[4]. Indeed, a recent longitudinal study of COVID-recovered, symptomatic individuals, published by the COVERSCAN study investigators, reveals that in this relatively young, low risk population 70% had impaired organ function 4 months later[4]. Treatment regimens to attenuate the initial infection, to reduce the severity of disease, and prevent its residual effects, constitute an urgent medical need.

The surface of SARS-CoV-2 virus particles is decorated with a characteristic 'crown' of spikes, formed of trimers of the spike (S) protein, which enable receptor-mediated plasma membrane fusion to enable viral entry into human cells, after priming by the host proteases furin and TMPRSS2[6,7], via an interaction between the surface of the spike receptor binding domain (RBD) and the cell surface angiotensin-converting enzyme-2 (ACE2) receptor. A furin protease cleavage site potentiates the infectivity of SARS-CoV-2[8], but mutations in and around the SARS-CoV-2 furin site are occasionally found in clinical isolates[9,10]. Laboratory passaged SARS-CoV-2 lacking a functional furin cleavage site fails to gain entry via membrane fusion via ACE2, and is instead capable of infection via ACE2 mediated endocytosis, albeit less efficiently, involving proteins such as NPC intracellular cholesterol transporter 1 (NCP1) and 2 that, are involved in endolysomal trafficking and membrane fusion[11]. Several cryo-EM structural studies have revealed that the spike adopts a mixed population of conformational states[12,13,14,15]. Our recent work[12] has established that the wild-type spike trimer contains a fatty acid binding site situated at each interface between two RBDs from adjacent subunits: in the resulting "locked" conformers, inter-subunit contacts between RBDs are maximised (Figure 1) such that a molecule of linoleate (LA), a nutritionally essential dietary fatty acid, is bound in each of three binding sites of the spike trimer. The K_d of LA^- for the isolated SARS-CoV-2 spike RBD has been determined by surface plasmon resonance as ~41nM[12]. Given that the interactions with the residues R408, Q409 and K417 from the adjacent chain in the trimer are not available in the isolated RBD, it is likely that LA^- has a higher affinity for the intact trimer. In contrast, in the 'open' states, one of the ACE2-binding domains (RBD) adopts a more extended, solvent exposed conformation. Crucially, the ACE2 interaction surfaces of the RBDs are occluded in the locked state and only available for receptor interaction in the more exposed, open states.

Figure 1. Inter-subunit contacts between RBDs are maximised in the locked spike.

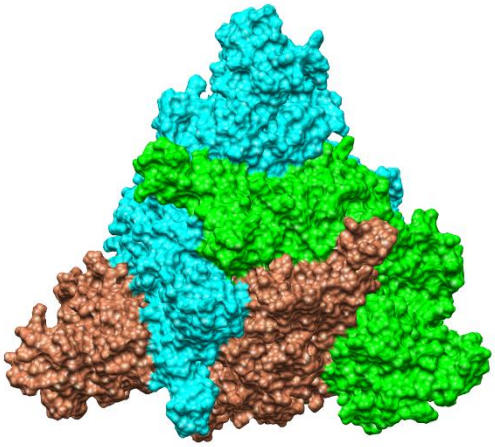

Top view of the locked conformation of the SARS-CoV-2 spike trimer with three linoleate molecules bound, following 200 ns of MD simulation, showing the close contacts between the subunits. Individual chains are shown in surface representation and coloured cyan, green and brown, respectively.

The spike protein fatty acid binding site[6] lies adjacent to a flexible hinge region beneath each of the RBDs and at its interface with neighbouring subunits. This hinge is believed to allow the large movement required to extend the RBD into an open conformation capable of binding ACE2. LA^- is bound with its hydrophobic tail nestled in a hydrophobic groove on the underside of the RBD from one chain, while the carboxylate head group moiety is within salt-bridging distance of two charged residues, R408 and K417, and hydrogen-bonding distance of Q409 on the adjacent RBD chain. The extensive LA^- interactions, involving two RBDs, in these locked structures support the conclusion that LA^- binding stabilises a condensed, locked state of the spike trimer. This proposal is supported by our observations of EM grids, where images suggest that ~70% of spike trimers on the EM grid adopt the locked form if exposed to LA, whereas only 30% are closed (all RBDs down) if fatty acids are lacking[13,14].

These observations led Toelzer *et al*. to hypothesise that stabilising the locked (ACE2-interaction-face occluded) conformation of the spike protein reduces the opportunity for receptor-mediated cell entry via interaction with ACE2[12]. The spike protein fatty acid pocket represents a potentially druggable site: this stabilization might therefore also be achieved by binding of high-affinity small molecule ligands: such ligands might potentially reduce cellular ingress by maintaining the spike protein in the locked conformation incompetent for ACE2 interaction. This proposal is supported by the finding that prior exposure to linoleate reduces SARS-CoV-2 replication in human epithelial cells[12].

In the light of these findings, we here investigate binding of LA^- and other ligands at the SARS-CoV-2 spike protein fatty acid binding site, using molecular simulations to explore the dynamic properties of the spike trimer in the apo (unliganded) state and in the LA-bound (holo) form in the locked and open conformations. Motivated by reports that the SARS-CoV-2 spike protein binds cholesterol[7], we also investigate the interactions of cholesterol with the fatty acid binding site. Furthermore, as cholesterol and the anti-inflammatory steroid dexamethasone (an agent demonstrated to improve outcomes for severely ill SARS-CoV-2 patients)[16] are chemically and structurally similar, we introduced dexamethasone into the fatty acid (FA) binding site to establish whether it too can be accommodated and retained there. Lastly, we used the Bristol University Docking Engine (BUDE)[17] to screen an approved drug library for candidate small molecule ligands able to bind the spike protein LA^- binding site in the locked conformation, and thus potentially stabilize the spike in a form less competent for ACE2 interaction. Virtual screening using BUDE identifies multiple compound classes, including naturally occurring and synthetic retinoids and steroids and the fat-soluble vitamins D, K and A, as candidate ligands for the spike fatty acid binding site. Our data suggest that a range of small molecule ligands, including pharmaceuticals and dietary components, and some compounds with known activity against SARS-CoV-2 replication *in vitro*, have the potential to bind to the SARS-CoV-2 spike protein, and may thereby be capable of influencing the conformational changes required for receptor binding and possibly modulating viral infectivity.

Results

Molecular Dynamics Simulations of Ligand Complexes of the Locked Form of the Spike

To investigate interactions of the SARS-CoV-2 spike fatty acid binding site with small molecule ligands, and the effects of the ligands on the spike and its dynamics, we performed molecular dynamics (MD) simulations of fatty-acid free 'apo' spike protein and its complexes with the de-protonated, charged form of linoleic acid (as it would be at physiological pH) linoleate(LA^-), cholesterol (previously proposed to bind to the SARS-CoV-2 spike), and the chemically and structurally similar anti-inflammatory agent dexamethasone (Figure 2). Dexamethasone is increasingly widely used as a therapeutic intervention for SARS-CoV-2-infected patients[16]. This work builds on our previously reported MD studies of LA^- binding[12]: we significantly extend the duration of simulations of the spike LA^- complex and expand our investigations to include additional candidate ligands.

In 200 ns MD simulations of the locked structures, starting from the cryo-EM structure (PDB code 6ZB5), the surrounding residues are ordered around the bound LA^- ligand (Figure 3A). The LA^- molecules themselves (Figure 4A) move very little within the fatty acid binding site (RMSD $\leq$ 3 Å). Hydrogen bonds of the LA^- linoleate head group with Q409, and salt bridge contacts with R408, are largely maintained; when the latter salt bridge is lost it is replaced by interactions with K417 (Figure S1). Comparison of overall Cα RMSD and by-residue RMSF plots of the uncomplexed and LA^--bound locked forms of the spike show that, while, on the timescale of these simulations, the overall dynamic properties of the spike trimer as a whole are little affected by LA^- binding (Figure 4D, E), the presence of ligand rigidifies the FA binding site (residues 330-480) as evidenced by the reduced fluctuations of residues surrounding the ligand (Figure 4H, I) and has an effect that extends towards the N-terminus as far as residue 310. In contrast, in simulations of the uncomplexed apo spike protein in the locked form, the fatty acid site exhibits comparatively greater fluctuations (Figure 4H) that lead to its eventual collapse.

As a starting point for explorations of the potential for other compounds to bind in the fatty acid binding site, and taking into account reports that the SARS-CoV-2 spike protein binds cholesterol[7], we next investigated the interactions of cholesterol within the FA site. Cholesterol was manually positioned in the FATTY ACID binding site by superposition onto the position of bound LA^- in the cryo-EM structure (PDB ID 6ZB5) after MD minimization, and oriented such that the polar end of cholesterol aligned with the LA^- linoleate head group and could replicate the inter-chain interactions made by LA^- bound to the spike trimer. All three cholesterol molecules remain bound to the closed spike trimer throughout three replicate 200 ns MD simulations (Figure 4B) with their hydroxyl moieties maintaining interactions with R408, Q409 and K417 in the FA binding site, as well as making occasional contacts with the threonine residues T415 and T373 (Figure 3B). Notably, the RMSD values for bound cholesterol appear lower than those for either LA^- (above) or dexamethasone (below) indicating that this ligand fits tightly into the spike FATTY ACID site.

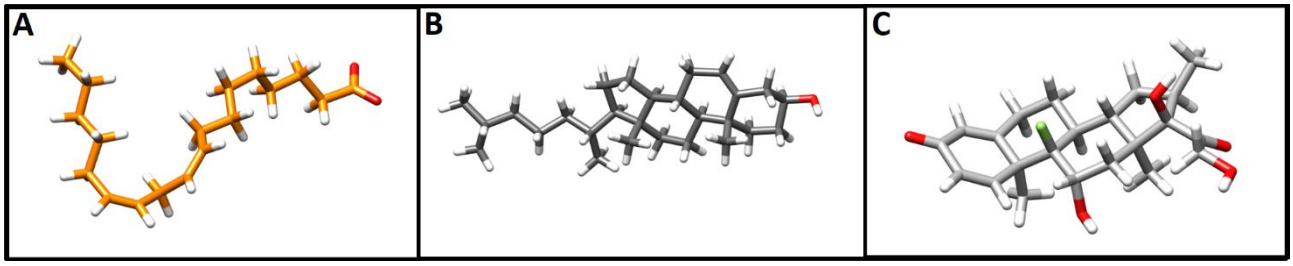

Figure 2 Structures of (A) linoleate; (B) cholesterol; and (C) dexamethasone from equilibrated simulations of complexes with the locked SARS-CoV-2 spike

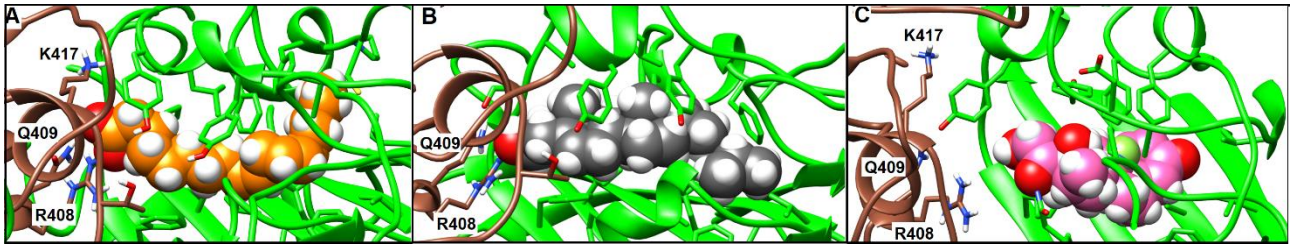

Figure 3. Representative structures of bound linoleate, cholesterol and dexamethasone following 200 ns of molecular dynamics simulations of complexes with the locked spike trimer. Brown and green ribbons denote different chains of the spike trimer (same color coding used throughout). **A**. Representative structure of bound linoleate (spheres, carbon atoms orange) after 200 ns MD simulation starting from the cryo-EM structure 6ZB5. Note the interactions of the linoleate head group with R408, Q409 and K417. **B**. Representative structure of cholesterol (spheres, carbon atoms grey) following simulation. **C**. Representative structure of dexamethasone (spheres, carbon atoms pink) after simulation in the locked spike trimer.

In order to further explore the potential for other ligands to bind in the spike fatty acid site, the synthetic corticosteroid dexamethasone, a compound structurally and chemically similar to cholesterol, was oriented in the fatty acid site as described above for cholesterol, and the complex subjected to 200 ns molecular dynamics simulations. During the three replicate simulations, all the dexamethasone molecules (three per spike trimer) remain bound. RMSD plots (Figure 4C) reveal that dexamethasone can move more freely within the fatty acid site than either bound LA^- or cholesterol and can sample a wider range of orientations due, probably because of its less extended structure (Figure 2C, 3C).

Comparison of Ca RMSD plots for simulations of the respective ligand complexes indicates that, compared to the apo form, binding of LA^- (Figure 4E), and, to a lesser extent, dexamethasone (Figure 4G), has a moderately stabilising effect on the locked conformation of the spike protein, as evidenced by reduced average Cα movements. However, one of the three simulations of the spike cholesterol complex (rep1, Figure 4F), appears to be somewhat destabilised, as shown by an increase in RMSD. This may reflect the more enclosed, constrained environment of cholesterol as a larger, rigid ligand within the fatty acid binding site (Figure 3B), which may favour opening of the pocket; flexion of bound cholesterol may transmit through the protein, via neighbouring secondary structure to disrupt more distant structural elements. In this simulation, residues 480–500 in chain B (directly above the fatty acid binding site), residues 620-630 in chains A and B, and residues 680–700 in chain B (containing the furin cleavage site) are also disrupted (Figure S2). Notably, the apparently globally destabilizing effect observed in this simulation of the cholesterol complex (Figure 4F) is not evident in simulations of the spike trimer in the apo , LA- or dexamethasone-bound forms (Figure 4D, E, G).

Comparison of by-residue RMSF plots for the four sets of simulations (Figure 4I - K) shows that the presence of any of the bound ligands reduces fluctuations in the region 330-480 corresponding to residues surrounding the fatty acid binding site, compared to the unliganded spike (Figure 4H). This stabilizing/rigidifying effect extends towards the N-terminus, as far as residue 310. Notably, despite the relative freedom of movement of bound dexamethasone, its presence rigidified the fatty acid binding site and its surroundings similarly to LA^- and cholesterol (Figure 4K).

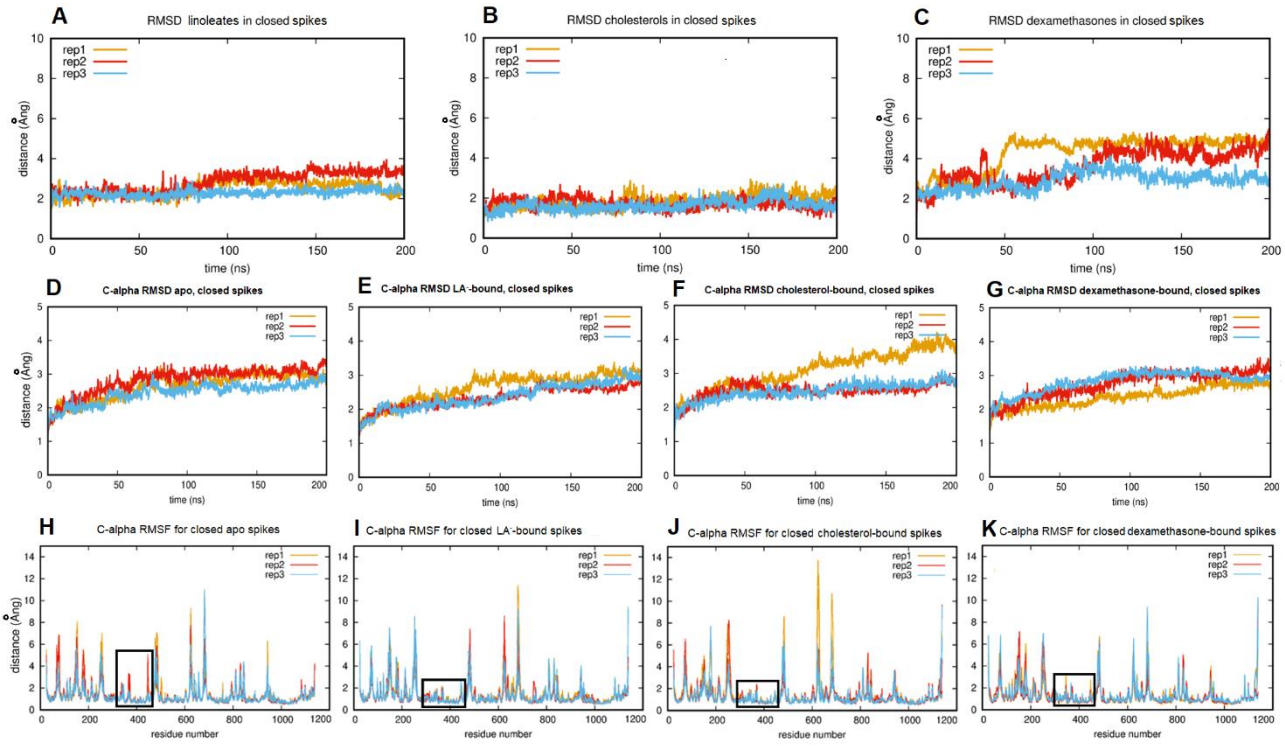

Figure 4. Ligand and protein dynamics during MD simulations of the locked spike trimer in apo and complexed forms. A, **B**, **C**: RMSD plots showing averaged ligand movement over time within binding sites for repeat simulations of (**A**) linoleate (**B**) cholesterol and (**C**) dexamethasone. Note the greater relative motion of dexamethasone. **D**, **E**, **F**, **G**: Cα RMSDs averaged over time for repeat simulations of the apo (unliganded) locked spike trimer (**D**) and of its complexes with LA^- (**E**), cholesterol (**F**) or dexamethasone (**G**). **H**, **I**, **J**, **K**: Cα RMSFs for repeat simulations of the apo (unliganded) locked spike trimer (**H**) and of its complexes with LA^- (**I**), cholesterol (**J**) and dexamethasone (**K**). Black rectangles indicate the fatty acid pocket and adjacent regions (residues 310 – 480) that are rigidified (reduced fluctuation) in simulations of the ligand complexes compared to the apo form.

Molecular Dynamics Simulations of Ligand Complexes of the Open Form of the Spike

In contrast to the locked form, cryo-EM structures of the spike protein in the partially open form are less well ordered, and bound LA^- was not readily resolved. Therefore, to explore possible interactions of LA^- with the spike protein in the partially open form, the locked spike trimer (PDB code 6ZB5[12]) was aligned with the open form and LA^- (positioned as in the locked structure) was placed into the open structure (Toelzer *et al*. Electron Microscopy Databank EMD-11146) such that interactions between the linoleate head group and residues R408, K417 and Q409 at the subunit interface could be maintained. Where this was not possible, the pose of bound LA^- was adjusted slightly to provide the potential for alternative hydrogen bonds or salt-bridging interactions to be made. This showed that the open conformation (EMD-11146), contains three distinct environments for the three bound LA^- molecules, that are referred to here as sites 1, 2 and 3. Site 1 is analogous to the LA^- binding site in the locked conformation, and retains the salt-bridge and hydrogen-bond interactions of the linoleate head group with R408, Q409 and K417 on the adjacent chain at the interface between RBDs. However, in the open form of the spike protein the presence of the RBD of one chain in a raised, open conformation disrupts the other two fatty acid binding sites. Thus, in site 2, the LA^- linoleate head group which, in the locked state, would associate with R408 and Q408 on the subunit opposite, instead contacts residues K386 and N388 from the same spike subunit, and, unlike site 1, does not make contacts that bridge the subunit interface. In site 3 bound LA^- associates with the underside of the RBD that is raised in the open conformation. LA^- binding at site 3 allows the linoleate head group to

interact across the domain interface with residues R408, Q409 and Q414 on the opposite chain and with K386 on the same chain, while residues F392, F515, L387, V382 and the disulphide C391-C525, interact with the hydrophobic LA^- tail.

This LA^--bound open complex was then subjected to 200 ns MD simulations, in triplicate. LA^- molecules bound in site 1 (equivalent to its binding site in the locked structure) maintain their original orientation and contacts during all repeat simulations. LA^-- bound in site 2 retains contacts with K386 and N388 at the rim of the binding site, but fails to make any interdomain connections. The behaviour of LA^- bound in site 3 is more dynamic. In two of the three replicate simulations, LA^- bound in site 3 migrates further from its starting position, but revisits the site regularly. However, in one of the repeat simulations, the LA^- molecule bound in site 3 begins to dissociate after 150 ns of MD (Figure S2). These results show weaker binding of LA^- to the SARS-CoV-2 spike protein in the open conformation, specifically at the binding site (site 3) that differs most from its equivalent in the locked form, and indicate a correlation between tight LA^- binding and closure of the RBD.

Complexes of the open form of the spike with cholesterol were then generated as above and subjected to three replicate 200 ns simulations. During these simulations all three cholesterol molecules remained bound to the spike trimer, with the behaviour of cholesterol bound at sites 1 and 2 similar to that observed for LA^- above. However, the behaviour of cholesterol bound in site 3 was noticeably different. In two of the three replica simulations, cholesterol bound in site 3 (i.e. associated with the open chain of the spike trimer) migrates to an alternative binding site (Figure 5B, circled in black) within the first 5 ns of the 200 ns trajectory, where it remains for the rest of the simulation. This alternative binding site is composed of prolines 330, 579 and 521 at the far end and lined with hydrophobic residues including the C525 - C391 disulphide, F329 and V327 (Figures 5B, 5D). Residues 318 to 326 and 588 to 595 have been identified as responsible for the rigid body rotation[18] of the RBD and 330 to 335 and 527 to 531 for the lift[18] required to enable the RBD to rise into a position that presents it for interaction with the ACE2 as highlighted in figure S4. Cholesterol binding at this alternative site 3 would probably restrict the motion required for full closure. In the third replicate simulation, cholesterol at site 3 also moves into this site, but binds in the opposite orientation with its more polar end towards the hydrophobic end of the binding site and is less stable. Altogether, these results indicate that cholesterol binds less tightly than LA^- at site 3, and that other sites in the open spike conformation may have higher affinity for this ligand.

We also performed 200ns MD simulations of dexamethasone bound to the open form of the spike protein, with three molecules of dexamethasone were modelled into the spike binding sites as described above. As for simulations with cholesterol (above), the behaviour of dexamethasone bound in sites 1 and 2 was analogous to that observed for LA. Dexamethasone bound in site 1 retained contact with R408, Q409 and K417, while dexamethasone bound in site 2 retained contact with N388 and the hydrophobic residues F377, F374 and Y365. Dexamethasone bound in site 3 was not stably bound, drifting further from its starting positions (Figure S5) and approaching, but not remaining near, the alternative binding site favoured by cholesterol (Figure 5C). Thus, over the duration of these simulations, dexamethasone did not locate a high affinity binding site close to the spike RBD in the open conformation These data indicate that dexamethasone does not have a favoured binding site around site 3 of the open spike, and does not make persistent interactions with the alternative cholesterol binding site (above) situated in the spike protein hinge region, though it may remain bound at the other fatty acid binding sites.

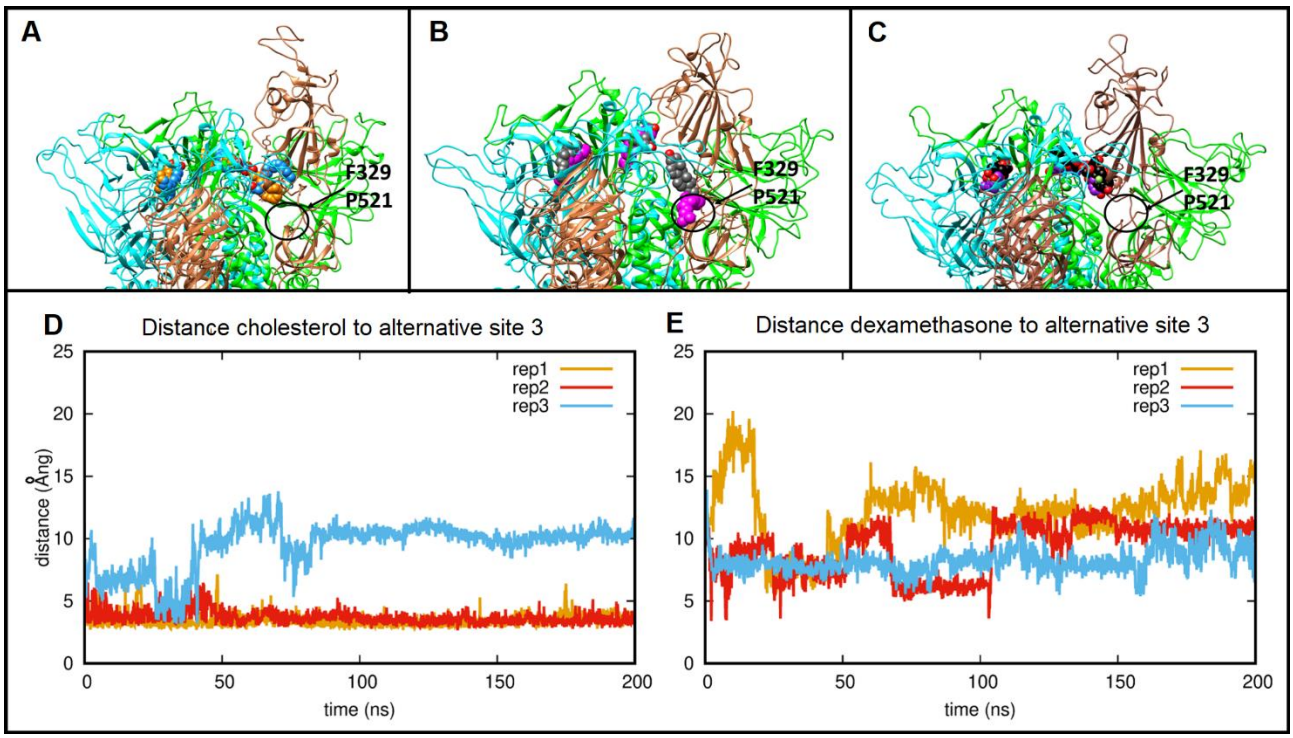

Figure 5. Ligand interactions of the SARS-CoV-2 spike protein in the open form. A. Starting (carbon atoms shown in yellow) and final (carbon atoms blue) positions of three LA^- molecules from a 200 ns MD simulation of their complex with the SARS-CoV-2 spike in the open conformation. **B.** Starting (carbon atoms grey) and final (carbon atoms magenta**)** positions of three cholesterol molecules from an equivalent 200 ns MD trajectory. **C.** Starting (carbon atoms black) and final (carbon atoms purple) positions of three dexamethasone molecules in the last frame of an equivalent 200 ns MD trajectory. A black circle (panels **A**, **B**, **C**) denotes the alternative binding site 3 sampled by the site 3 cholesterol (see main text). **D, E.** Time-dependence of distance between the site 3 cholesterol (**D**) or dexamethasone (**E**) and residues F329 and P521 of the alternative site 3 favoured by cholesterol in the hinge region.

Virtual Ligand Screening at the Locked SARS-CoV-2 Spike Protein Fatty Acid Binding Site

The identification of a binding pocket for free fatty acids in the SARS-CoV-2 spike protein[12] led us to explore the possibility of this site as a target for binding of approved drugs (Figure 6A - D). Accordingly, we used the Bristol University Docking Engine (BUDE[17]) to screen *in silico* a library of existing approved drugs that are potential candidates for repurposing against COVID-19. As the starting structure for docking, we chose an equilibrated frame from MD simulations of the spike trimer in the locked, LA-bound form described above (hereafter cryo-EM_{eq}), because this structure had side chains optimally oriented to form salt-bridges and hydrogen bonds with the linoleate head group (LA^- is treated throughout as linoleate, as above). BUDE results were filtered on the basis of ligand size, such that compounds having < 15 or > 45 heavy atoms were eliminated. The remaining compounds were then ranked based on their predicted binding affinity (BUDE energy) and the single best conformer for compounds scoring ≤ –100 kJ/mol was selected for more detailed analysis. The list of compounds ranked in this way is given in Supplementary Information (Table S2).

The presence of LA^- in the repurposing library allows for validation of BUDE docking by comparison of the predicted mode of LA^- binding and that observed in the equilibrated structure of the locked complex (i.e. the cryo-EM_{eq} structure). Experimentally, the K_d of LA^- for the isolated SARS-CoV-2 spike RBD has been determined by surface plasmon resonance as ~41nM[12]. LA^- ranked 86th in the list of compounds ordered by BUDE binding energy, with a heavy atom RMSD between the docked (highest scoring pose from BUDE) and the cryo-EM_{eq} LA^- of 1.6 Å. Furthermore, in the cryo-EM_{eq}

structure, and as described above, the linoleate carboxylate group forms multiple electrostatic interactions with the side chains of R408 and Q409. In the lowest-energy docked pose generated by BUDE, the linoleate carboxylate group occupies the same position as that observed in the cryo-EM_{eq} structure and forms multiple electrostatic interactions with the R408 and Q409 side chains (Figure 6E). Thus, the positions of bound LA^- in the experimental and docked structures are very similar, so we consider that their close correspondence, and the consistency in their interactions between experimental and MD data, provides support for the use of BUDE in this virtual screening study.

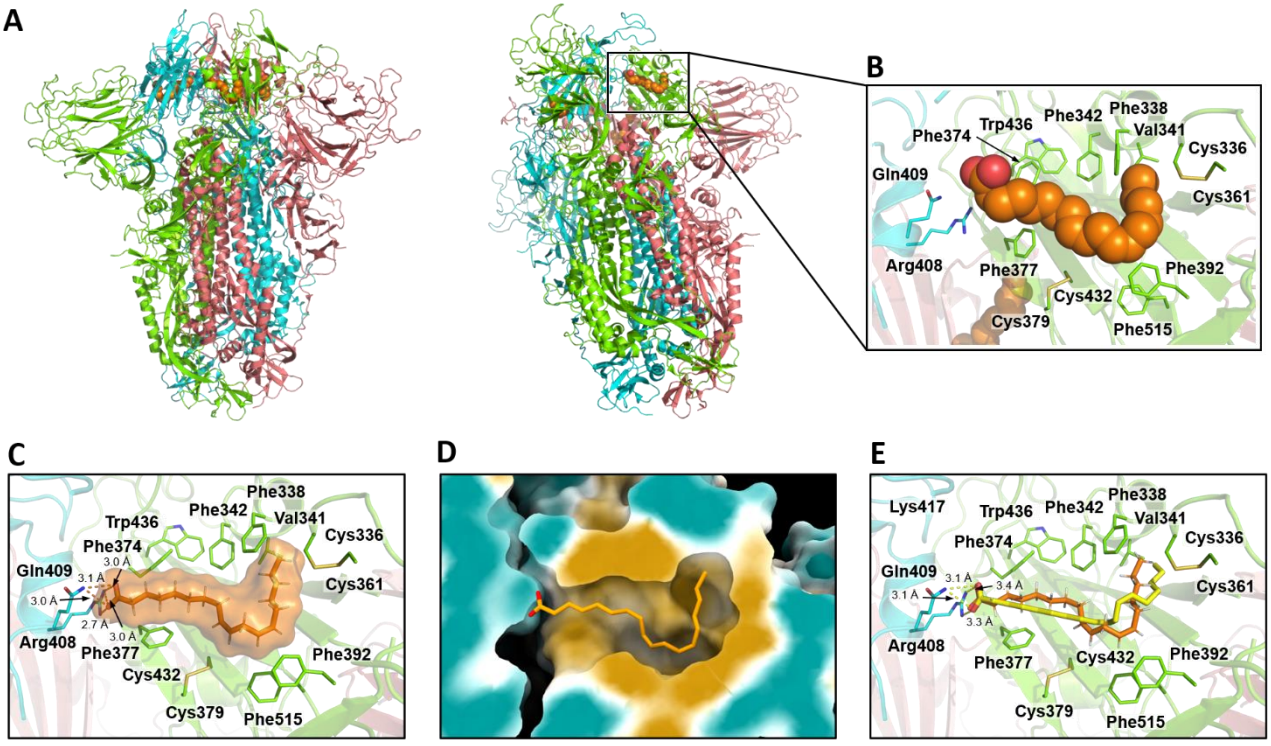

Figure 6. BUDE docks linoleate into the locked SARS-CoV-2 spike trimer in a conformation consistent with cryo-EM structures. A. Cryo-EM structure of LA-bound spike trimer in the locked conformation. **B**. View of LA^- binding site in the same structure. **C**. LA^- binding pose in the structure used for docking (i.e. the cryo-EM structure after MD equilibration). **D**. Surface representation of the LA^- binding pocket in this structure, coloured according to hydrophobicity: cyan for most hydrophilic though white to gold for most hydrophobic. The linoleate binding mode after equilibration by MD is shown as sticks. **E**. Superimposition of the BUDE predicted linoleate binding pose (yellow) and equilibrated structure (brown). The overall RMSD between the two poses is 2.2 Å.

Inspection of the lists of highly ranked ('hit') compounds ordered by BUDE energy (Table S2) or ligand efficiency (Table S3) identified a number of compound classes that can be considered to be of particular interest, based upon their demonstrated or proposed relevance to SARS-CoV-2 and/or other respiratory viral infections. Notably, the fat-soluble vitamins D (vitamin D3 metabolite calcitriol), K and A are all present in the FDA library and all rank more highly than LA^- by calculated BUDE binding energy. Indeed, vitamin K2 is the highest ranked compound in the BUDE output list, with vitamin A acetate ranked 17th by predicted binding energy, vitamin D (calcitriol) 24th, vitamin A 38th and vitamin K1 70th. Inspection of the respective lowest energy BUDE docked poses showed that all of these vitamins align very well with the pose adopted by LA^- stably bound to the locked spike trimer after 200 ns of MD simulation (Figure 7). In the case of calcitriol (Figure 7A, D) and vitamin K2 (Figure 7B, E), the presence of double bonds in their extended side chains allows them to align closely with the hydrophobic LA^- tail and consequently to fit well into the highly hydrophobic FA binding site.

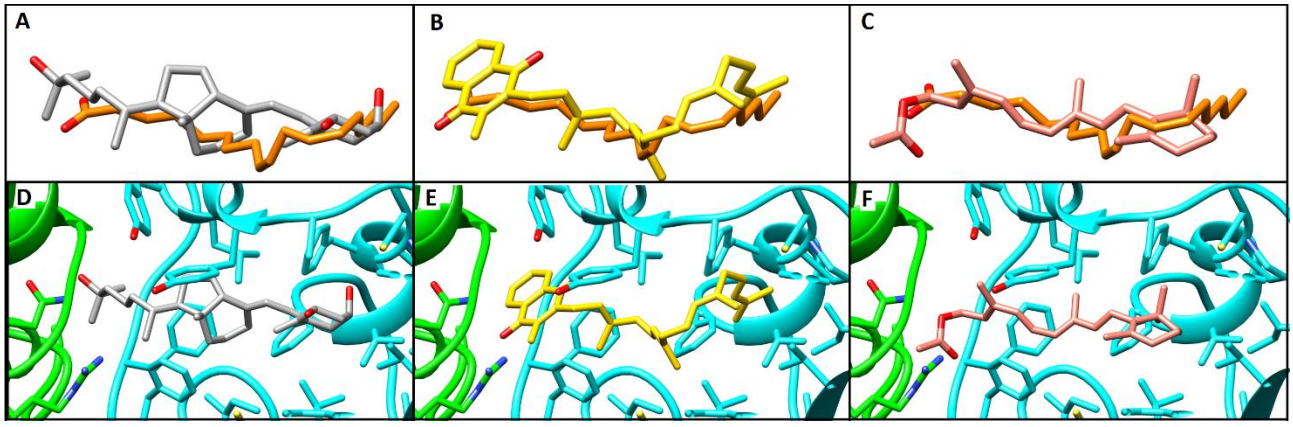

Figure 7. Docked poses of vitamins in the fatty acid binding site of the SARS-CoV-2 spike. Overlays are shown of LA^- (carbon atoms in orange, structure after MD simulation of the locked spike complex) with the lowest energy conformations from BUDE docking of: **A** calcitriol (vitamin D, carbon atoms grey); **B** vitamin K2 (carbon atoms yellow); and **C** vitamin A acetate (carbon atoms salmon). Panels **D, E** and **F** show the docked positions in the LA^- site of: **D** vitamin D; **E** vitamin K2; and **F** vitamin A acetate.

Numerous studies have sought to identify candidate approved drugs suitable for repurposing as therapies for COVID-19, both computationally and experimentally. Notably, Riva et al.[19] screened ~12000 compounds from the ReFRAME library[20] for inhibition of SARS-CoV-2 replication in Vero E6 cells. Accordingly, we then compared the list of highly ranked compounds from the BUDE screen against those identified by Riva et al.[19] as able to inhibit viral replication. Of the 100 agents on their list of most active compounds three: tretinoin, acitretin and tazarotene, are relatively prominent in the ordered list of compounds identified by BUDE, ranking 5th, 8th, and 214th, respectively by BUDE energy. According to Riva et al[19], acitretin at 2.5 μM inhibits viral replication by 40 %, while tazarotene and tretinoin at 1 μM inhibit viral replication by 50% and 42%, respectively. Notably, the lowest energy binding poses identified by BUDE for all of these compounds involve electrostatic interactions with R408 and Q409, in addition to hydrophobic interactions with the remainder of the binding pocket (Figure 7A, C, D). These data suggest that these compounds may act on viral replication by binding to this free fatty acid site in a manner similar to LA.

Like vitamin A, tretinoin, acitretin and tazarotene are all retinoic acid receptor agonists: tretinoin (atralin) is also known as all-trans retinoic acid, acitretin is a second-generation retinoid and tazarotene (avage) is classed as a third-generation retinoid. In their recent study Riva[19] highlight retinoic acid receptor agonists as one of 15 target classes that were enriched in their assay, with a total of 13 retinoic acid receptor agonists appearing in their list of 100 top-ranked active compounds. With this in mind, we then interrogated the list of BUDE hits to seek additional retinoid compounds, and, in addition to vitamin A, identified a further four retinoids: adapalene (9th, third-generation topical retinoid), fenretinide (10th, synthetic phenylretinamide retinol analogue), etretinate (18th, second-generation retinoid) and isotretinoin (68th, 13-cis retinoic acid) as prominent among the highly ranked hits. Thus, virtual screening by BUDE identifies multiple synthetic retinoids in addition to vitamin A as candidate ligands, supporting the contention that the spike protein LA^- site may also be capable of binding members of this class of compounds.

Similarly, reports that the spike protein binds cholesterol[21] as well as the possibility that the LA^- site may be capable of binding dexamethasone (above), motivated scrutiny of the lists of BUDE hits for steroid compounds. A variety of steroid agents, including progestins (hydroxyprogesterone caproate, ranked 29th by BUDE energy, chlormadinone acetate (41st), and medroxyprogesterone acetate (50th)); androgens (testosterone enanthate, 19th); corticosteroids (methylprednisolone hemisuccinate, 47th);

bile acids (ursolic acid, glycocholic acid, dehydrocholic acid; 6th, 7th and 49th, respectively) and the synthetic androstane steroid abiraterone acetate (23rd); all feature among candidate ligands that are highly ranked by BUDE. Several other steroid-like natural products (carbenoxolone (2nd), oleanolic acid (30th), madecassic acid (35th) and hederagenin (37th)) are also prominent in the BUDE ranking list. Although (and typical of the results of docking studies) the lists of hits are subject to some variation with the different ranking procedures, there is a consistent preponderance of steroids among the most highly ranked compounds.

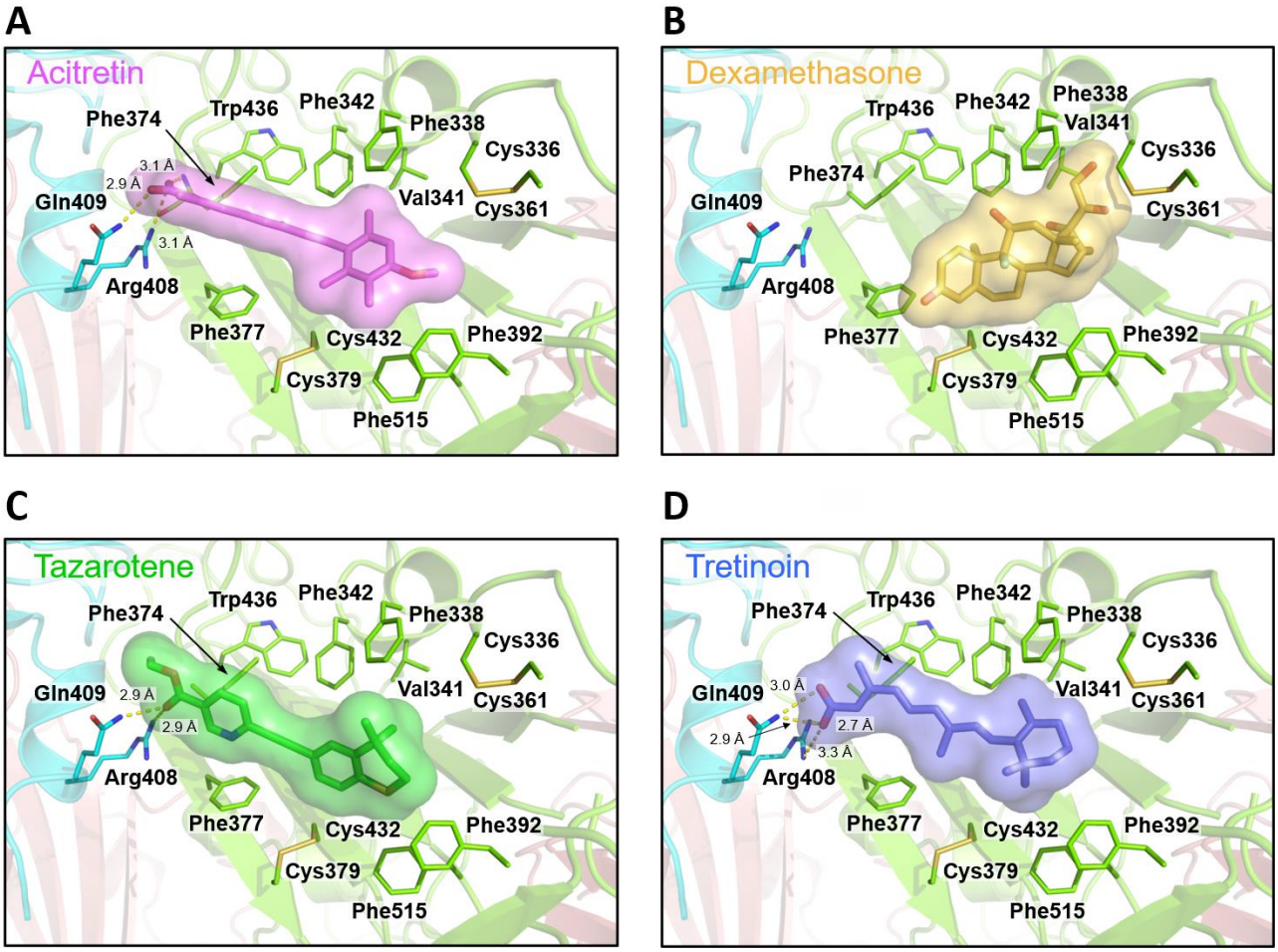

Figure 8. Docked poses of FDA-approved drugs in the free fatty acid binding pocket. In all cases, the highest scoring pose is shown. **A.** Acitretin (purple). **B.** Dexamethasone (orange). **C.** Tazarotene (green) **D.** Tretinoin (blue). Electrostatic interactions are shown as dashed yellow lines.

As described above, the anti-inflammatory corticosteroid dexamethasone has attracted considerable attention on the basis of its demonstrated efficacy improving outcomes for COVID-19 patients in clinical trials[16]. Accordingly, we also considered the position of dexamethasone in the results of BUDE virtual screening. Unlike LA^- and the retinoic acid receptor agonists, but consistent with the MD simulations described above, the dexamethasone binding mode predicted by BUDE does not involve interactions with R408 or Q409 and instead is dominated by hydrophobic interactions with residues on the opposite side of the binding site (Figure 7B). Thus, although other steroidal compounds score more highly, our docking data also support the molecular dynamics simulations described above in identifying a possible interaction of dexamethasone with the SARS-CoV-2 spike protein.

Taken together, therefore, the results of this virtual screening of the SARS-CoV-2 spike protein fatty acid binding site provide evidence that this represents a possible interaction site for both physiological and synthetic ligands, including fat-soluble vitamins, retinoids and steroids.

Discussion

The unexpected discovery of a fatty acid binding site in locked structures of the SARS-CoV-2 spike protein trimer, and the subsequent inference that LA^- binding at this site stabilizes a locked conformation of the spike that is less competent for ACE2 receptor binding, raises the possibility that small molecule ligands binding at this site might modulate the conformation of the spike and disrupt the process of SARS-CoV-2 infection by preventing ACE2 receptor binding. Accordingly, we have sought to explore these hypotheses, and extend our previous structural studies, by investigating the dynamic properties of the spike trimer in different conformations (locked and open) and in complex with LA^- and other potential ligands identified from the literature; and by running a virtual screen in an effort to identify further small molecule ligands from an approved drug library.

The results reported here support our previous findings that LA^- makes persistent and stable interactions with the SARS-CoV-2 spike in its locked form. Furthermore, by-residue RMSF plots (Figure 4) indicate that, compared to the uncomplexed form of the protein, the locked spike has locally reduced mobility when LA^- is bound. The conclusion that the fatty acid binding site is rigidified by bound ligand is corroborated by the observations that the fatty acid site collapses in MD simulations of the unliganded (apo) structure, and is also collapsed in available cryo-EM structures of the spike in its apo form[13]. Together with the observation that LA^- in the binding site that involves the repositioned subunit of the spike trimer in the open form (site 3) is more mobile and can on occasion dissociate, these data provide evidence that the locked form of the spike is stabilized by LA^- binding. Notably, the region stabilised by ligand occupation of the fatty acid site extends beyond the immediate fatty acid binding site as far as residue 310, that in turn contacts portions of the spike protein known to influence infectivity. Specifically, these include position 614 (the site of the widespread D614G mutation that increasingly predominates in circulating SARS-CoV-2 strains[22]) and the furin cleavage site (residues 680-6) important in activation of the spike to enable interaction with ACE2 in lung cells[23].

We then investigated the possibility that the spike fatty acid binding site may interact with ligands other than LA. In particular, we investigated whether it may be a binding site for cholesterol, given that the spike protein has previously been demonstrated to bind cholesterol[21], and the accumulating evidence associating individuals with elevated cholesterol levels with enhanced viral infectivity and adverse patient outcomes[24,25]. Also, the similarity of dexamethasone to cholesterol, and its importance in COVID-19 treatment, motivated us to also consider dexamethasone as a possible ligand for the fatty acid site. Both cholesterol and dexamethasone could be readily positioned in the locked LA^- site and remained bound to the locked form of the spike during simulations on the timescales investigated here (200 ns). However, the increase in the average Cα RMSD observed for one of the replicate simulations indicated that cholesterol binding has a greater, and potentially destabilising, effect on the structure of the locked spike than either LA^- or dexamethasone. Moreover, in two of the three replicate simulations of cholesterol bound to the spike in the open state, cholesterol in the site formed by the open subunit (site 3, above) migrates to an alternative site in the open structure that is not sampled by LA^- or dexamethasone. The proximity of this site to the hinge region, which is important for conformational changes of the spike between the locked and open forms[26], provides a possible mechanism by which cholesterol binding at this position may affect the dynamics and preferred conformation of the spike RBD, potentially stabilising an orientation which favours RBD presentation for potential ACE2 binding.

Increasing evidence connects cholesterol levels with COVID-19 disease risk and outcomes. For example, the apolipoprotein (apo)E4 genotype is associated with increased risk for severe COVID-19[27] and with increased circulating cholesterol[28]. The use of cholesterol lowering statins reduces the risk of developing severe COVID and reduces recovery time in less severe cases[29]. Cholesterol has been proposed to promote SARS-CoV-2 infection by multiple mechanisms including promoting ACE2 and furin trafficking to viral entry points[24], but plasma levels are reduced in patients with established disease and correlate inversely with disease severity[21,30,31]. Our data are consistent with previous observations of cholesterol binding by the spike protein, and therefore, when considered together with those findings, suggest possible additional involvement of cholesterol in infection, i.e. through binding to the spike. Cholesterol binding by the spike protein could constitute a sequestration mechanism that maintains local, cellular cholesterol at a level that supports continued infectivity in the face of a reduction in blood levels. Alternatively, it is possible that cholesterol bound to the spike protein may be more directly involved in the infection process, potentially through effects on the spike conformation and presentation of the RBD for interaction with ACE2 (see above). Additional involvement of cholesterol in virus entry is also likely in the case of circulating spike variants lacking a functional furin cleavage site[11] that may alternatively utilise an endosomal entry mechanism[31], as evidenced by identification of genes such as the host cholesterol transporter NPC1 as essential to cell killing by such strains[11].

In silico screening of a library of approved drugs against the locked form of the SARS-CoV-2 spike protein yielded numerous candidates for ligands that may bind to the fatty acid pocket. Importantly, our chosen docking tool, BUDE, identified LA^- as a high-scoring ligand that binds in a conformation similar to that observed experimentally, providing some initial validation of our approach. Furthermore, comparison of the lists of BUDE hits with the results of experimental screening studies of approved drugs, suggests that some compounds known to be active against SARS-CoV-2 replication in cultured cells may bind to this site. Moreover, the BUDE screen also identified the fat-soluble vitamins D, K and A, present in our approved drug library, as potential ligands that may stabilise the locked form of the SARS-CoV-2 spike by binding to the fatty acid site. Notably, the vitamin D3 metabolite calcitriol was recently identified as able to reduce viral titres in infected monkey and human nasal epithelial cell lines[32]. Alongside socio-economic deprivation[33], evidence is accumulating that deficiencies in at least two of these vitamins (D and K) are associated with increased risk of developing severe COVID-19[34,35]. Although we are unaware of any demonstrated link between population vitamin A levels and COVID-19 risk, we note the heavy COVID-19 burden in some regions where vitamin A deficiency may be prevalent[36]. Aside from the role of vitamin D in modulating the host immune response to respiratory infections[37], our data then suggest that, as for cholesterol (above), sequestration through binding to the SARS-CoV-2 spike protein is a possible mechanism by which vitamin levels are reduced during COVD-19 disease. Furthermore, the implication that, by binding to the spike FA site, fat-soluble vitamins can stabilise the locked form of the spike and actively inhibit viral entry suggests that these compounds could also play a more direct role in protecting host cells from viral infection. This possible involvement of micronutrients in countering SARS-CoV-2 highlights the potential for food poverty as a risk factor for COVID-19 disease. These possibilities are worthy of further investigation.

In addition to vitamin A, retinoids[38] were highly represented in the lists of candidate hit compounds identified by BUDE. Three retinoids, acitretin, tazarotene and tretinoin, have recently been shown to inhibit SARS-CoV-2 replication in VeroE6 cells[19], with a further four (adapalene, fenretinide, etretinate and isotretinoin (13-cis retinoic acid)) also prominent in the BUDE ranking lists. Retinoids have been proposed as candidates for inclusion in COVID-19 treatment regimes, particularly in combination with type 1 interferons (IFN-I[39]), but this is based upon their ability to upregulate host antiviral responses, rather than any hypothesized direct effect upon viral entry or replication. Coronaviruses such as SARS-CoV and MERS-CoV are known for their ability to disrupt IFN-I signalling (for review see ref[40]). Moreover, recent *in vitro* data identify SARS-CoV-2 as more

susceptible than SARS-CoV to the IFN-I response[41,42], although results from the WHO SOLIDARITY trial[43] did not reveal any benefits from subcutaneous interferon-β1a for hospitalised COVID-19 patients. It has been suggested that IFN-I administration may be most effective as a prophylactic or early treatment option; thus agents such as retinoids that may stimulate secretion of, and potentiate response to, IFN-I remain worthy of investigation. Our data provide additional motivation for such studies by suggesting that, through binding to the fatty acid pocket and keeping the spike protein in the locked conformation that does not interact with ACE2, retinoids may act by directly affecting viral entry, particularly early in the infection process, as well as via upregulation of the host antiviral response. Literature searches identified a single clinical trial (NCT04353180) of a retinoid (isotretinoin/13-cis retinoic acid) as a treatment for COVID-19, but this remains at an early stage[44].

Virtual screening using BUDE also identifies several steroid drugs as potential candidate ligands for the fatty acid binding pocket. This is of particular interest because recent meta analysis[45] has confirmed that corticosteroids other than dexamethasone, namely methylprednisolone and hydrocortisone, were also beneficial to critically ill COVD-19 patients, as measured by 28-day all-cause mortality, in randomised clinical trials[45]. Although steroids are not prominent in compound lists recovered from cell-based screens of approved drugs, and compounds for which clinical trial data are available (dexamethasone, methylprednisolone and hydrocortisone) are not the highest-scoring such agents on the BUDE ranking lists (respectively 273rd, 47th (hemisuccinate), 266th and 97th on the BUDE energy rankings), they feature highly in the virtual screening output. When considered together with the results of the MD simulations described above, which support stable interactions of dexamethasone with the spike fatty acid pocket, this suggests that corticosteroids that are observed experimentally to be effective against SARS-CoV-2 or COVID-19 may have an additional mode of action involving direct interaction with the spike, as well as their better characterized effects on the host response.

It is important to emphasise that we make no claims regarding the possible clinical efficacy of compounds identified in the virtual screening described here. No recommendation on treatment should ever be based on the results of modelling alone. However, the interactions that we identify suggest that compounds known from experimental evidence to be active against SARS-CoV-2 replication in cultured cells may interact with the spike fatty acid binding site, and that this interaction may be responsible for some of their observed antiviral activity.

Conclusions

In summary, we here report extensive computational investigations of the interactions of small molecule ligands with the fatty acid binding site of the SARS-CoV-2 spike in its locked and open forms. MD simulations indicate that the physiological ligand LA^- is able to stabilize the locked form of the spike, but binds more weakly to the exposed fatty acid site of the open form. In contrast, cholesterol, which is also retained by the locked spike conformation, is not retained by the fatty acid site of the open spike. Indeed, the propensity of cholesterol to migrate to a distinct site, situated in the hinge region that connects the spike RBD to the remainder of the protein, suggests the possibility that interactions with cholesterol may modulate conformational changes in the SARS-CoV-2 spike and, potentially, promote the infection process. Moreover, despite the similarity between dexamethasone and cholesterol, they behave differently under these simulation conditions. Our MD simulations and docking experiments find that dexamethasone may also bind to the fatty acid site and stabilise the locked conformation. We suggest that dexamethasone binding to the SARS-CoV-2 spike may represent an additional contribution to its efficacy in treating COVID-19 disease.

In silico screening of the locked spike against a library of approved drugs was validated by the identification of LA^- as a high-ranking hit, with a mode of binding that replicates that observed

experimentally. Our docking study identifies vitamins A, D and K as additional candidates for binding to the spike fatty acid site and as such potentially capable of stabilising the spike in the locked conformation, suggesting that further study is warranted to explore whether vitamins play a more direct role than previously envisaged in protecting against SARS-CoV-2 infection. In addition to vitamin A, three further retinoids that are known inhibitors of SARS-CoV-2 replication in cell-based infection models are predicted to bind the spike fatty acid site in a similar fashion to LA, supporting our previous contention that stabilising the locked spike reduces infectivity. Docking experiments, as well our MD simulations, also indicate that dexamethasone is capable of binding to the SARS-CoV-2 spike, and further that the fatty acid pocket may bind a range of other natural and synthetic steroids in addition to dexamethasone or cholesterol. These findings therefore suggest that, in addition to their effects on host response, certain vitamins, retinoids and steroids may also affect SARS-CoV-2 via direct binding to the spike protein, supporting further investigation of these classes for possible activity against COVID-19. Experiments to explore and validate these hypotheses are now underway.

Acknowledgments

We thank BrisSynBio, a BBSRC/EPSRC Synthetic Biology Research Centre (Grant Number: BB/L01386X/1) for funding DKS and the HPC BlueGem and EPSRC vis HECBIOSIM (hecbiosim.ac.uk) for providing ARCHER time through a COVID-19 rapid response call. AJM, JS and CKC thank the British Society for Antimicrobial Chemotherapy (grant number BSAC-COVID-30). AJM thanks EPSRC (grant number EP/M022609/1, CCP-BioSim) for support. CS and IB are supported by the Wellcome Trust (210701/Z/18/Z; 106115/Z/14/Z) and the BBSRC (BB/P000940/1). This work used computational facilities of the Advanced Computing Research Centre, University of Bristol, http://www.bris.ac.uk/acrc/. We also thank Oracle Research for Oracle Public Cloud Infrastructure (https://cloud.oracle.com/en_US/iaas) time under an award for COVID-19 research and the Elizabeth Blackwell Institute, University of Bristol, for their support.

Methods

Molecular Dynamics Simulations

Proteins were prepared as described in Toelzer[12]. Loops for the unstructured regions of the locked (LA^-- bound) and open (apo) cryo-EM structures were built using Chimera (UCSF)[46]. Likely disulphide bonds were reconstructed based on experimentally observed distances (42 for the locked structure and 43 for the open) and each chain sequence was used in an EBI-blast check to verify wild type Spike sequence post build. Procheck[47] was then used to check the quality of the resulting structure prior to simulation. Acpype[48] was used to prepare the topologies for all ligands. Cholesterol and dexamethasone were superimposed onto the equilibrated LA^- positions with most polar ends of the molecules oriented to the carboxylate position of the linoleate. Dexamethasone and cholesterol were fitted into the fatty acid binding pocket in the locked conformations following a brief relaxation with LA^-.

Simulation details: All simulations were performed under the Amber99SB-ildn[49,50,51] forcefield in NPT ensembles at 310 K using periodic boundary conditions. Hydrogen atoms, consistent with pH7, were added to the complex. Short-range electrostatic and van der Waals interactions were truncated at 1.4 nm while long range electrostatics were treated with the particle-mesh Ewald method and a long-range dispersion correction applied. A simulation box extending 2 nm from the protein was filled with TIP3P water molecules and 150 mM Na^+ and Cl^- ions added to attain a neutral charge overall. Pressure was controlled by the Berendsen barostat and temperature by the V-rescale thermostat. The simulations were integrated with a leapfrog algorithm over a 2 fs time step, constraining bond vibrations with the P-LINCS method. Structures were saved every 0.1 ns for analysis in each of the simulations over 100 ns. Simulations were run on the Bristol supercomputer BlueCrystal 4, the BrisSynBio BlueGem, and the UK supercomputer, ARCHER.
Software: The GROMACS-2019.2[52] suite of software was used to set up and perform the molecular dynamics simulations and analyses for BlueGem and BlueCrystal runs and the ARCHER runs. Molecular graphics manipulations and visualisations were performed using VMD-1.9.1[53] and Chimera-1.10.2[46].

Virtual Screening of Ligands

A database of 2697 FDA-approved drugs in SDF format was downloaded from SelleckChem (https://www.selleckchem.com/). 3D coordinates of each compound were generated using The Open Babel Package, version 2.3.2 (http://openbabel.org)[55], and up to 50 conformers per compound were produced using Confort[54] (Tripos Inc.). The receptor used for docking was an equilibrated frame from the molecular dynamics simulation of the LA^-- bound SARS-CoV-2 spike glycoprotein cryo-EM structure (PDB code 6ZB5, 2.85 Å resolution). A 13 Å radius around LA^- was selected as the docking pocket with C9 being the centroid. LA^- was subsequently removed prior to the docking calculations. The virtual screen was run using BUDE1.2.9[17] via a cloud computing platform powered by Oracle Corp. The total number of compounds screened was 2505 (Table S1), accounting for 39 compounds that had undefined atoms, and 153 compounds with atoms that are not parameterised in the BUDE forcefield.

References

1. Johns Hopkins Coronavirus Resource Center. 2020. *COVID-19 Map - Johns Hopkins Coronavirus Resource Center*. [online] Available at: <https://coronavirus.jhu.edu/map.html> [Accessed 22 September 2020].
2. Mehta, P., McAuley, D., Brown, M., Sanchez, E., Tattersall, R. and Manson, J., 2020. COVID-19: consider cytokine storm syndromes and immunosuppression. The Lancet, 395(10229), pp.1033-1034.
3. Puntmann, V., Carerj, M., Wieters, I., Fahim, M., Arendt, C., Hoffmann, J., Shchendrygina, A., Escher, F., Vasa-Nicotera, M., Zeiher, A., Vehreschild, M. and Nagel, E., 2020. Outcomes of Cardiovascular Magnetic Resonance Imaging in Patients Recently Recovered From Coronavirus Disease 2019 (COVID-19). *JAMA Cardiology*
4. Dennis, A., Wamil, M., Kapur, S., Alberts, J., *et al*. Multi-organ impairment in low-risk individuals with long COVID. medRxiv preprint doi:https://doi.org/10.1101/2020.10.14.20212555 .
5. Yelin, D., Wirtheim, E., Vetter, P., Kalil, A., Bruchfeld, J., Runold, M., Guaraldi, G., Mussini, C., Gudiol, C., Pujol, M., Bandera, A., Scudeller, L., Paul, M., Kaiser, L. and Leibovici, L., 2020. Long-term consequences of COVID-19: research needs. *The Lancet Infectious Diseases*. Published online 01.09.2020.
6. Shang, J., Wan, Y., Luo, C., Ye, G., Geng, Q., Auerbach, A. and Li, F., 2020. Cell entry mechanisms of SARS-CoV-2. *Proceedings of the National Academy of Sciences*, 117(21), pp.11727-11734.
7. Walls, A., Park, Y., Tortorici, M., Wall, A., McGuire, A. and Veesler, D., 2020. Structure, Function, and Antigenicity of the SARS-CoV-2 Spike Glycoprotein. Cell, 181(2), pp.281-292.e6. https://doi.org/10.1016/j.cell.2020.02.058
8. Xia, S., Lan, Q., Su, S., Wang, X., Xu, W., Liu, Z., Zhu, Y., Wang, Q., Lu, L. and Jiang, S., 2020. The role of furin cleavage site in SARS-CoV-2 spike protein-mediated membrane fusion in the presence or absence of trypsin. Signal Transduction and Targeted Therapy, 5(1).**5,** 92 (2020). https://doi.org/10.1038/s41392-020-0184-0
9. Xing, Y., Li, X., Gao, X. and Dong, Q., 2020. Natural Polymorphisms Are Present in the Furin Cleavage Site of the SARS-CoV-2 Spike Glycoprotein. Frontiers in Genetics, 11. https://doi.org/10.3389/fgene.2020.00783
10. Liu, Z., Zheng, H., Lin, H., Li, M., Yuan, R., Peng, J., Xiong, Q., Sun, J., Li, B., Wu, J., Yi, L., Peng, X., Zhang, H., Zhang, W., Hulswit, R., Loman, N., Rambaut, A., Ke, C., Bowden, T., Pybus, O. and Lu, J., 2020. Identification of Common Deletions in the Spike Protein of Severe Acute Respiratory Syndrome Coronavirus 2. Journal of Virology, 94(17).
11. Zhu, Y., Feng, F., Hu, G., Wang, Y., Yu, Y., Zhu, Y., Xu, W., Cai, X., Sun, Z., Han, W., Ye, R., Chen, H., Ding, Q., Cai, Q., Qu, D., Xie, Y., Yuan, Z. and Zhang, R., 2020. The S1/S2 boundary of SARS-CoV-2 spike protein modulates cell entry pathways and transmission. bioRxiv preprint doi: https://doi.org/10.1101/2020.08.25.266775
12. Toelzer C, Gupta K, Yadav SKN et al. (2020) Free fatty acid binding pocket in the locked structure of SARS-CoV-2 spike protein. *Science*. 21.09.2020 DOI:10.1126/science.abd3255
13. Wrapp, D., Wang, N., Corbett, K., Goldsmith, J., Hsieh, C., Abiona, O., Graham, B. and McLellan, J., 2020. Cryo-EM structure of the 2019-nCoV spike in the prefusion conformation. Science, 367(6483), pp.1260-1263.
14. Tortorici, M.A., Walls, A.C., Lang, Y. et al. Structural basis for human coronavirus attachment to sialic acid receptors. Nat Struct Mol Biol 26, 481–489 (2019). https://doi.org/10.1038/s41594-019-0233-y
15. Yuan, Y., Cao, D., Zhang, Y., Ma, J., Qi, J., Wang, Q., Lu, G., Wu, Y., Yan, J., Shi, Y., Zhang, X. and Gao, G., 2017. Cryo-EM structures of MERS-CoV and SARS-CoV spike glycoproteins reveal the dynamic receptor binding domains. *Nature Communications*, 8(1).
16. The RECOVERY Collaborative Group. Dexamethasone in Hospitalized Patients with Covid-19 — Preliminary Report. Online ahead of print. NEJM 2020 DOI: 10.1056/NEJMoa2021436
17. McIntosh-Smith, S., Price, J., Sessions, R. and Ibarra, A., 2014. High performance in silico virtual drug screening on many-core processors. *The International Journal of High Performance Computing Applications*, 29(2), pp.119-134.

18. Melero, R., Sorzano, COS., Foster, B., Vilas J-L., Martínez M. et al Continuous flexibility analysis of SARS-CoV-2 Spike prefusion structure. bioRxiv preprint doi: https://doi.org/10.1101/2020.07.08.191072
19. Riva, L., Yuan, S., Yin, X. et al. Discovery of SARS-CoV-2 antiviral drugs through large-scale compound repurposing. Nature (2020). https://doi.org/10.1038/s41586-020-2577-1
20. Jeff Janes, Megan E Young, Emily Chen, Nicole H Rogers, Sebastian Burgstaller-Muehlbacher, Laura D Hughes, Melissa S Love, Mitchell V Hull, Kelli L Kuhen, Ashley K Woods, Sean B Joseph, H Michael Petrassi, Case W McNamara, Matthew S Tremblay, Andrew I Su, Peter G Schultz, Arnab K Chatterjee. The ReFRAME library as a comprehensive drug repurposing library and its application to the treatment of cryptosporidiosis. *PNAS* 115, 42, 10750-10755.
21. Peng, Y., Wan, L., Fan, C., Zhang, P., Wang, X., Sun, J., Zhang, Y., Yan, Q., Gong, J., Yang, H., Yang, X., Li, H., Wang, Y., Zong, Y., Yin, F., Yang, X., Zhong, H., Cao, Y. and Wei, C., 2020. Cholesterol Metabolism--Impacts on SARS-CoV-2 Infection Prognosis. medRxiv preprint doi: https://doi.org/10.1101/2020.04.16.20068528
22. Korber B., Fischer, WM., Gnanakaran S., LaBranche, CC., Saphire, EO., Montefior, DC. Tracking Changes in SARS-CoV-2 Spike: Evidence that D614G Increases Infectivity of the COVID-19. 2020, Cell 182, 812-827. doi.org/10.1016/j.cell.2020.06.04
23. Hoffmann et al., A Multibasic Cleavage Site in the Spike Protein of SARS-CoV-2 Is Essential for Infection of Human Lung Cells. 2020, Molecular Cell 78, 779–784 doi.org/10.1016/j.molcel.2020.04.022
24. Wang, H., Yuan, Z., Pavel, M., Hobson, R. and Hansen, S., 2020. The role of high cholesterol in age-related COVID19 lethality. doi: https://doi.org/10.1101/2020.05.09.086249
25. Zaki, N., Alashwal, H. and Ibrahim, S., 2020. Association of hypertension, diabetes, stroke, cancer, kidney disease, and high-cholesterol with COVID-19 disease severity and fatality: A systematic review. *Diabetes & Metabolic Syndrome: Clinical Research & Reviews*, 14(5), pp.1133-1142.
26. Henderson, R., Edwards, R.J., Mansouri, K. et al. Controlling the SARS-CoV-2 spike glycoprotein conformation. Nat Struct Mol Biol 27, 925–933 (2020). https://doi.org/10.1038/s41594-020-0479-4
27. Kuo, C., Pilling, L., Atkins, J., Masoli, J., Delgado, J., Kuchel, G. and Melzer, D., 2020. APOE e4 Genotype Predicts Severe COVID-19 in the UK Biobank Community Cohort. *The Journals of Gerontology: Series A* glaa131, https://doi.org/10.1093/gerona/glaa131
28. Saito, M., Eto, M., Nitta, H., Kanda, Y., Shigeto, M., Nakayama, K., Tawaramoto, K., Kawasaki, F., Kamei, S., Kohara, K., Matsuda, M., Matsuki, M. and Kaku, K., 2004. Effect of Apolipoprotein E4 Allele on Plasma LDL Cholesterol Response to Diet Therapy in Type 2 Diabetic Patients. *Diabetes Care*, 27(6), pp.1276-1280.
29. Daniels, L., Sitapati, A., Zhang, J., Zou, J., Bui, Q., Ren, J., Longhurst, C., Criqui, M. and Messer, K., 2020. Relation of Statin Use Prior to Admission to Severity and Recovery Among COVID-19 Inpatients. The American Journal of Cardiology. http://doi.org/10.1016/j.amjcard.2020.09.012
30. Wei, X., Zeng, W., Su, J., Wan, H., Yu, X., Cao, X., Tan, W. and Wang, H., 2020. Hypolipidemia is associated with the severity of COVID-19. Journal of Clinical Lipidology, 14(3), pp.297-304.
31. Hu, Xingzhong and Chen, Dong and Wu, Lianpeng and He, Guiqing and Ye, Wei, Low Serum Cholesterol Level Among Patients with COVID-19 Infection in Wenzhou, China (February 21, 2020). Available at SSRN: https://ssrn.com/abstract=3544826 or http://dx.doi.org/10.2139/ssrn.3544826
32. Mok, CK., Ng, YL., Ahidjo, BA., et al. Calcitriol, the active form of vitamin D, is a promising candidate for COVID-19 prophylaxis. BioRxiv preprint doi:https://doi.org/10.1101/2020.06.21.162396
33. Patel, J.A. Poverty, inequality and COVID-19: the forgotten vulnerable. Royal Society for Public Health 183 (2020) 110e111. https://doi.org/10.1016/j.puhe.2020.05.006
34. Benskin L. A. Basic Review of the Preliminary Evidence That COVID-19 Risk and Severity Is Increased in Vitamin D Deficiency . Frontiers in Public Health 2020 8 513 DOI=10.3389/fpubh.2020.0051
35. Dofferhoff, ASM., Piscaer, I., Schurgers, LJ., Visser, MJP. Reduced vitamin K status as a potentially modifiable risk factor of severe COVID-19, Clinical Infectious Diseases, ciaa1258, https://doi.org/10.1093/cid/ciaa1258

36. Akhtar, S., Ahmed, A., Randhawa, MA., Atukorala, S., Arlappa, N. et al. Prevalence of Vitamin A Deficiency in South Asia: Causes, Outcomes, and Possible Remedies. J Health Popul. Nutrition 2013 31(4):413-423
37. Greiller CL., Martineau AR. Modulation of the Immune Response to Respiratory Viruses by Vitamin D. Nutrients 2015, 7, 4240-4270; doi:10.3390/nu7064240
38. Thompson, B., Katsanis, N., Apostolopoulos, N. et al. Genetics and functions of the retinoic acid pathway, with special emphasis on the eye. Hum Genomics 13, 61 (2019). https://doi.org/10.1186/s40246-019-0248-9
39. Trasino SE. A role for retinoids in the treatment of COVID-19? Clin Exp Pharmacol Physiol. 2020;47:1765–1767DOI: 10.1111/1440-1681.13354
40. Park A., Iwasaki A. Type I and Type III Interferons –Induction, Signaling, Evasion, and Application to Combat COVID-19. Cell Host & Microbe 2020 27 (6) 870-878 DOI:https://doi.org/10.1016/j.chom.2020.05.008
41. Lokugamage KG., Hage A., de Vries M. et al. Type I interferon susceptibility distinguishes SARS-CoV-2 from SARS-CoV.J. Virol. doi:10.1128/JVI.01410-20
42. Mantlo E., Bukreyevaa N., Maruyamaa J., Paesslera S., Huang C. Antiviral Research 179 2020, 104811. https://doi.org/10.1016/j.antiviral.2020.104811
43. WHO Solidarity trial consortium. Repurposed antiviral drugs for COVID-19–interim WHO SOLIDARITY trial results. MedRxiv preprint https://doi.org/10.1101/2020.10.15.20209817
44. Clinicaltrials.gov. 2020. Assessment The Activity Value Of Isotretinoin (13- Cis-Retinoic Acid) In The Treatment Of COVID-19 (Randomized) - Full Text View - Clinicaltrials.Gov. [online] Available at: <https://clinicaltrials.gov/ct2/show/NCT04353180> [Accessed 22 September 2020].
45. The WHO Rapid Evidence Appraisal for COVID-19 Therapies (REACT) Working Group. Association Between Administration of Systemic Corticosteroids and Mortality Among Critically Ill Patients With COVID-19 A Meta-analysis. JAMA. 2020;324(13):1330-1341. doi:10.1001/jama.2020.17023
46. Chimera UCSF Chimera - a visualization system for exploratory research and analysis. Pettersen EF, Goddard TD, Huang CC, Couch GS, Greenblatt DM, Meng EC, Ferrin TE. J Comput Chem. 2004 Oct;25(13):1605-12. http://www.cgl.ucsf.edu/chimera
47. Laskowski R A, MacArthur M W, Moss D S, Thornton J M (1993). PROCHECK - a program to check the stereochemical quality of protein structures. J. App. Cryst., 26, 283-291.
48. AW Sousa da Silva and WF Vranken. ACPYPE - AnteChamber PYthon Parser interfacE. BMC Research Notes 5, 367 (2012).
49. GAFF Wang, J., Wolf, R. M.; Caldwell, J. W.;Kollman, P. A.; Case, D. A. "Development and testing of a general AMBER force field". J. Comput. Chem., 25, 2004, 1157-1174.
50. Amber D.A. Case, T.E. Cheatham, III, T. Darden, H. Gohlke, R. Luo, K.M. Merz, Jr., A. Onufriev, C. Simmerling, B. Wang and R. Woods. (2005) "The Amber biomolecular simulation programs." J. Comput. Chem. 26, 1668-1688.
51. Amber99SB-ildn Lindorff-Larsen K, Piana S, Palmo K, et al. Improved side-chain torsion potentials for the Amber ff99SB protein force field. Proteins. 2010;78(8):1950–1958. doi:10.1002/prot.22711
52. Gromacs Computer Physics Communications, Volume 91, Issues 1–3, 2 September 1995, Pages 43-56, GROMACS: A message-passing parallel molecular dynamics implementation https://doi.org/10.1016/0010-4655(95)00042-E
53. VMD Humphrey, W., Dalke, A. and Schulten, K., VMD - Visual Molecular Dynamics. J. Molec. Graphics, 1996, vol. 14, pp. 33-38.
54. Pearlman RS, Balducci R Confort User Manual. Distributed by Cetara, Princeton, NJ., U.S.A JChem. http://www.chemaxon.com/products/jchembase
55. N M O'Boyle, M Banck, C A James, C Morley, T Vandermeersch, and G R Hutchison. "Open Babel: An open chemical toolbox." *J. Cheminf.* 2011, 3, 33. DOI:10.1186/1758-2946-3-33

Supplementary Information

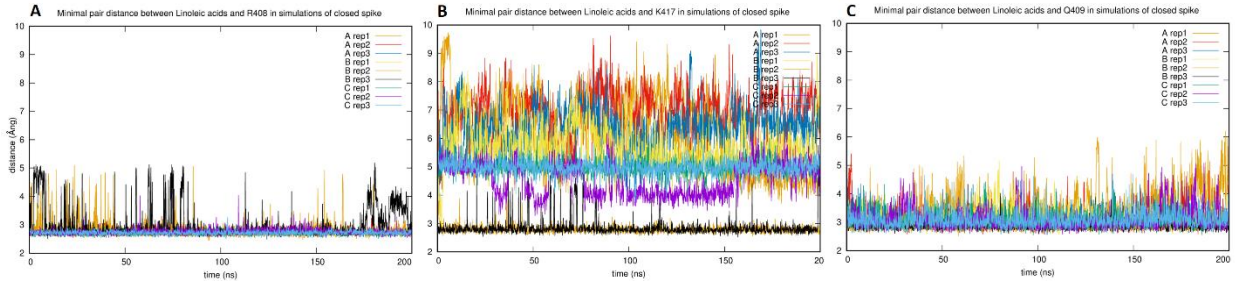

Figure S1. Interaction of linoleate with spike RBD during MD simulations of the locked complex. Plots show the minimal pairwise distances between linoleate atoms and A. the nitrogens of the R408 guanidinium, B. the nitrogen of the K417 amino group and C. the nitrogen and oxygen of Q409 amide (C) during simulations of locked linoleate bound complexes. Coloring of individual chains/replicates is consistent across the Figure.

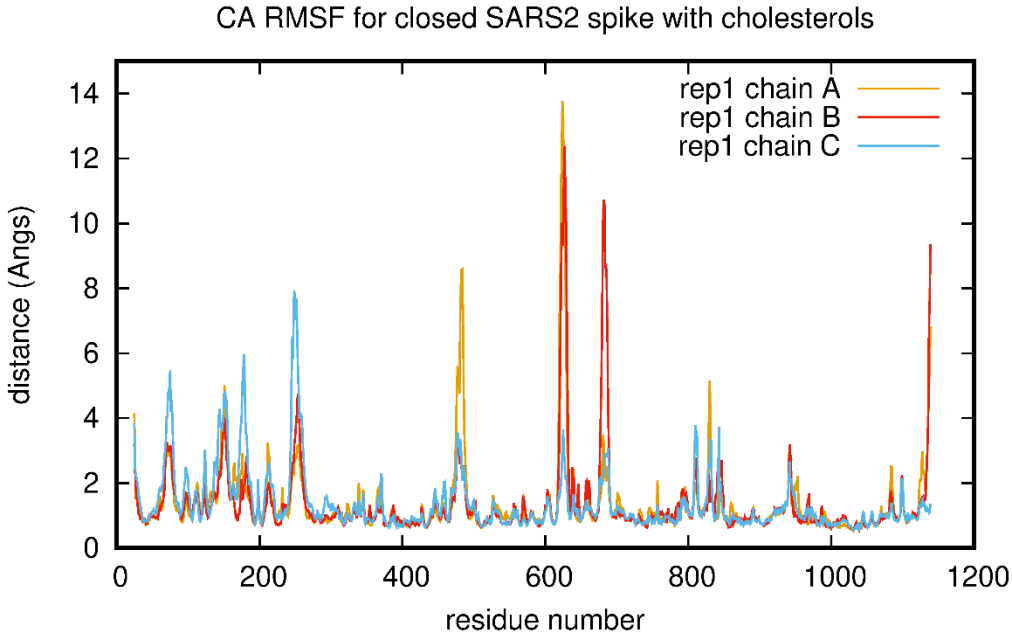

Figure S2. RMSF for the individual chains showing the regions destabilised by the binding of cholesterol in the fatty acid binding site.

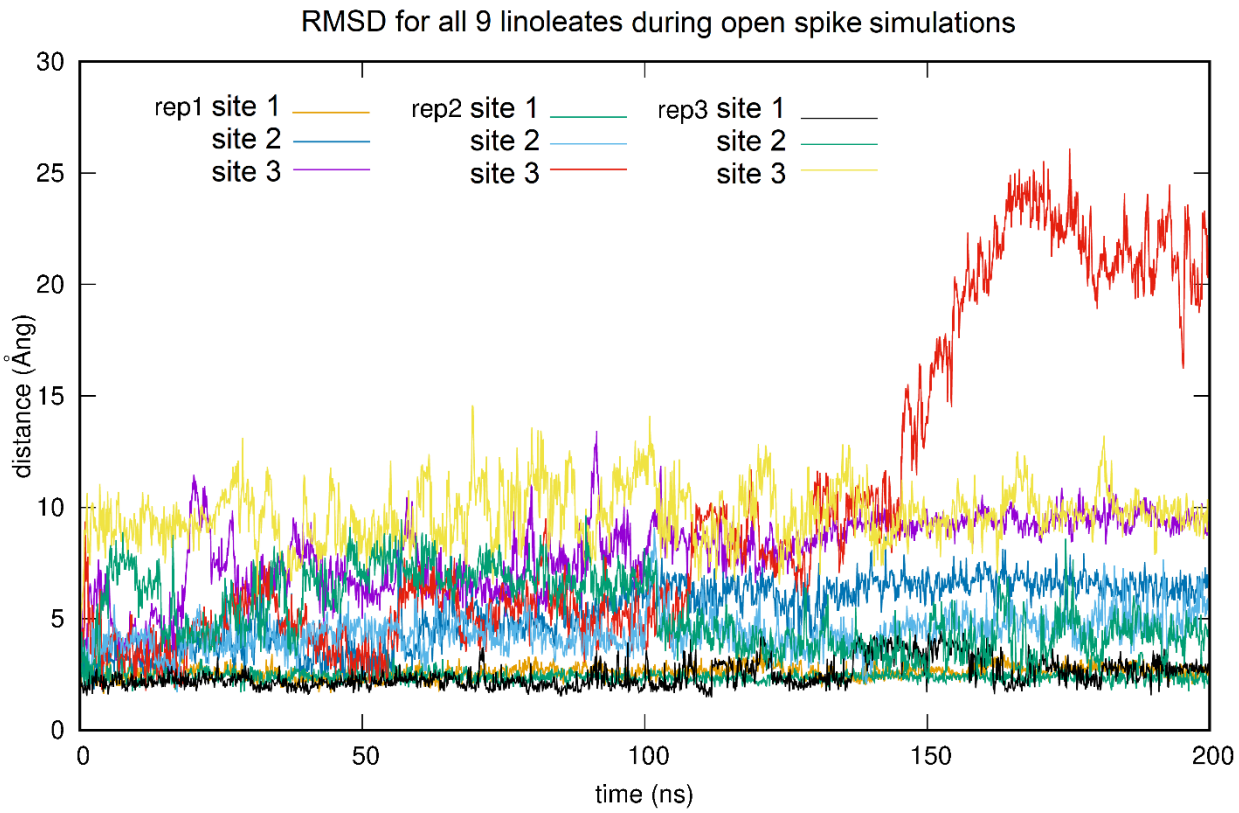

Figure S3. Stability of linoleate binding in simulations of the open spike. Figure shows mean distance moved by linoleate molecules from their positions in the starting structures during simulations. The C-alphas for the individual chains were aligned with those in their first frame and the distance calculated for linoleate compared to its coordinate position in the first frame, for each of 3 sites (site 1 = locked, site 2 = closed, site 3 = open as described earlier) during three replicate simulations of the open spike trimer. Note increased distance of LA^- in site 3 (open site) from its starting position (yellow, magenta traces), with dissociation evident in one trajectory (red trace).

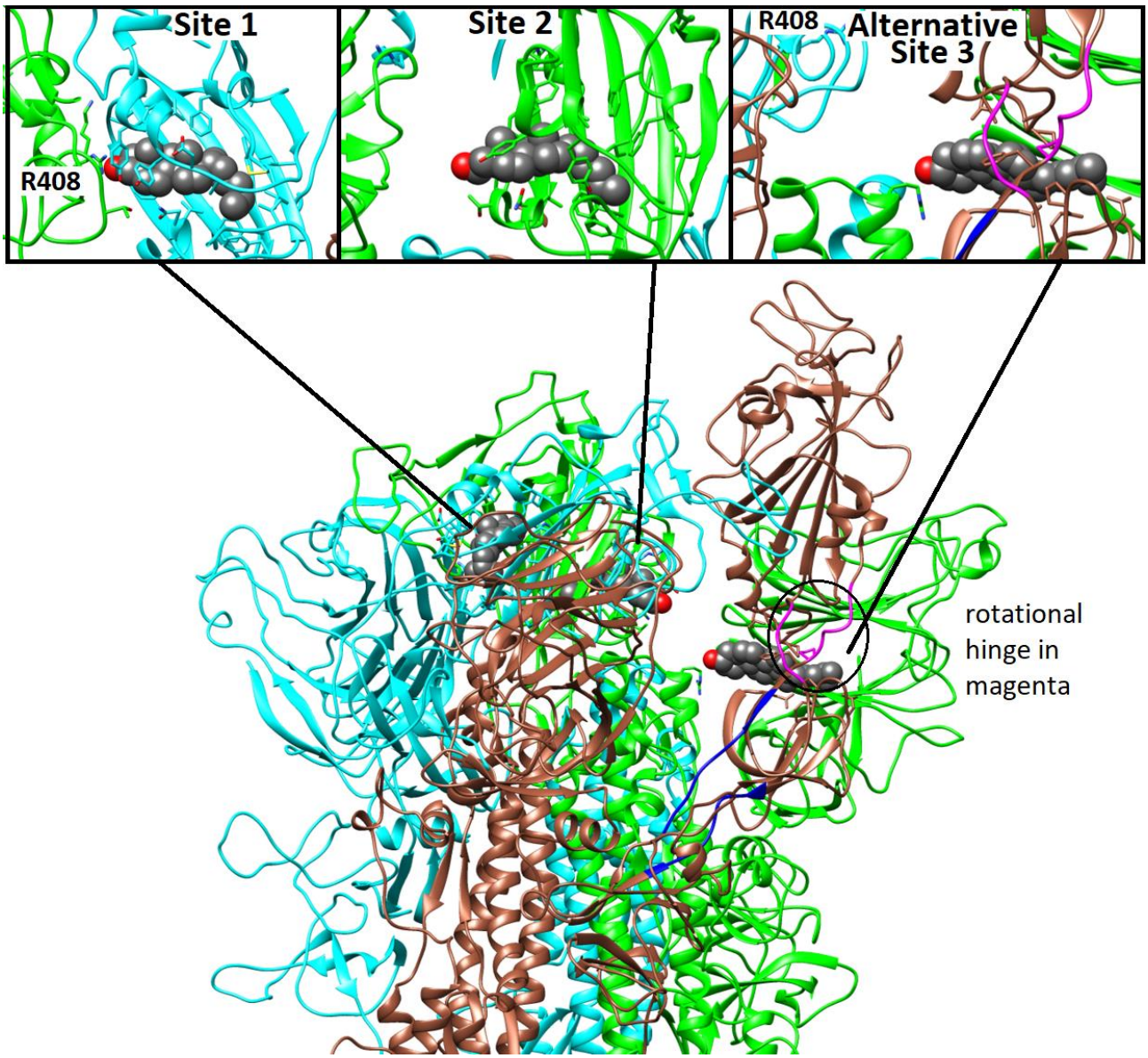

Figure S4. Three distinct cholesterol binding sites in the open spike conformation suggested by MD simulations. Figure shows SARS-CoV-2 spike chains A (cyan ribbon) B (brown ribbon) and C (green ribbon) with bound cholesterols (carbon atoms grey spheres) from the last frame of a 200 ns MD trajectory of the open SARS-CoV-2 spike trimer. Top row inserts illustrate cholesterol binding sites 1 and 2 and the alternative site 3. Main image shows relative positions of the three sites. Alternative site 3 is shown in the context of residues required for the rigid body rotational (circled and magenta ribbon) and vertical motion (dark blue ribbon) necessary to raise the RBD[18] for interaction with the ACE2 receptor.

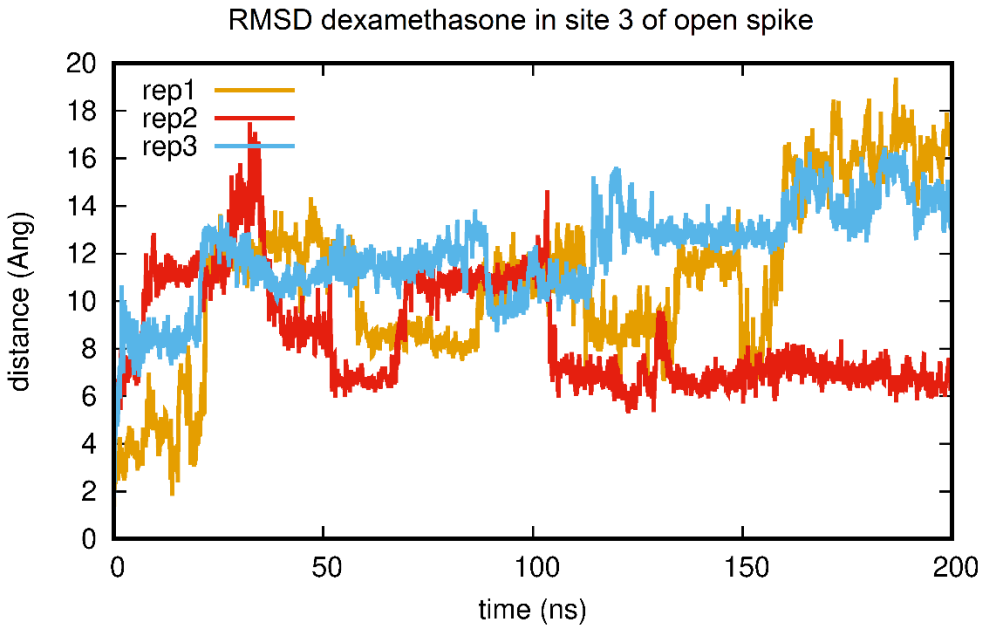

Figure S5. RMSD for dexamethasone bound to site 3 during MD simulations of the open spike complex. Plot shows RMSD of dexamethasone with respect to its position in site 3 of the starting structure (associated with the underside of the raised RBD).

SI Table S1.